The discovery of an M4+T8.5 binary system

Ben Burningham,[1][*] D. J. Pinfield,[1] S. K. Leggett,[2] C. G. Tinney,[3] M. C. Liu,[4][†]
D. Homeier,[5] A. A. West,[6] A. Day-Jones,[1] N. Huelamo,[7] T. J. Dupuy,[3] Z. Zhang,[1]
D. N. Murray,[1] N. Lodieu,[8] D. Barrado y Navascués,[7] S. Folkes,[1] M. C. Galvez-Ortiz,[1]
H. R. A. Jones,[1] P. W. Lucas,[1] M. Morales Calderon[7] and M. Tamura[9]

[1]*Centre for Astrophysics Research, Science and Technology Research Institute, University of Hertfordshire, Hatfield AL10 9AB*
[2]*Gemini Observatory, 670 N. A'ohoku Place, Hilo, HI 96720, USA*
[3]*University of New South Wales, Sydney, NSW 2052, Australia*
[4]*Institute for Astronomy, University of Hawai'i, 2680 Woodlawn Drive, Honolulu, HI 96822, USA*
[5]*Institut fur Astrophysik, Georg-August-Universitat, Friedrich-Hund-Platz 1, 37077 Gottingen, Germany*
[6]*MIT Kavli Institute for Astrophysics and Space Research, 77 Massachusetts Avenue, Cambridge MA 02139*
[7]*Laboratorio de Astrofísica Espacial y Física Fundamental, INTA, PO Box 78, E–28691 Villanueva de la Canada (Madrid), Spain*
[8]*Instituto de Astrofísica de Canarias, 38200 La Laguna, Spain*
[9]*National Astronomical Observatory, Mitaka, Tokyo 181-8588, Japan*

ABSTRACT

We report the discovery of a T8.5 dwarf, which is a companion to the M4 dwarf Wolf 940. At a distance of $12.50^{+0.75}_{-0.67}$ pc, the angular separation of 32 arcsec corresponds to a projected separation of 400 au. The M4 primary displays no Hα emission, and we apply the age–activity relations of West et al. to place a lower limit on the age of the system of 3.5 Gyr. Weak Hα absorption suggests some residual activity, and we estimate an upper age limit of 6 Gyr. We apply the relations of Bonfils et al. for $V - K_s$ and M_{K_s} to determine the metallicity, [Fe/H] $= -0.06 \pm 0.20$ for Wolf 940A, and by extension the T8.5 secondary, Wolf 940B. We have obtained *JHK* NIRI spectroscopy and *JHKL'* photometry of Wolf 940B, and use these data, in combination with theoretical extensions, to determine its bolometric flux, $F_{\rm bol} = 1.75 \pm 0.18 \times 10^{-16}$ W m^{-2}, and thus its luminosity $\log(L_*/L_\odot) = -6.07 \pm 0.04$. Using the age constraints for the system and evolutionary structural models of Baraffe et al., we determine $T_{\rm eff} = 570 \pm 25$ K and $\log g = 4.75 - 5.00$ for Wolf 940B, based on its bolometric luminosity. This represents the first determination of these properties for a T8+ dwarf that does not rely on the fitting of T dwarf spectral models. This object represents the first system containing a T8+ dwarf for which fiducial constraints on its properties are available, and we compare its spectra with those of the latest very cool BT–Settl models. This clearly demonstrates that the use of the $(W_J, K/J)$ spectral ratios (used previously to constrain $T_{\rm eff}$ and $\log g$) would have overestimated $T_{\rm eff}$ by $\sim$100 K.

Key words: surveys – stars: low-mass, brown dwarfs.

1 INTRODUCTION

The advent of the most recent generation of large imaging surveys (e.g. Lawrence et al. 2007; Delorme et al. 2008b and soon the VISTA surveys) has facilitated the identification of brown dwarfs with later spectral types (STs) than the latest T dwarfs found using Two-Micron All-Sky Survey (2MASS), DENIS or Sloan Digital Sky Survey (SDSS). For example, the UKIRT (United Kingdom Infrared Telescope) Infrared Deep Sky Survey (UKIDSS)

Large Area Survey (LAS; see Lawrence et al. 2007), which as of Data Release 4 (DR4) probes nearly three times the searchable volume of 2MASS for such objects, contains at least four T dwarfs with STs later than T8 (in addition to that identified in this work), which have recently been classified by Burningham et al. (2008): the T9 dwarfs ULAS J003402.77−005206.7 (ULAS 0034), CFBDS J005910.90−011401.3 (CFBDS 0059) and ULAS J133553.45+113005.2 (ULAS 1335); and the T8.5 dwarf ULAS J123828.51+095351.3 (ULAS 1238) (Warren et al. 2007; Delorme et al. 2008a; Burningham et al. 2008). The physical properties of these objects have been estimated by fitting various model spectra to near- and mid-infrared (IR) data (where available). Effective temperature ($T_{\rm eff}$) estimates vary from as cool as 500–550 K for

ULAS 1335 (Leggett et al. 2009) to as warm as 600–650 K for ULAS 0034 (Warren et al. 2007). Since parallax determinations are not yet available for these objects, these estimates are somewhat uncertain, based as they are on early generations of atmospheric models that are still under development. Also, current indications are that surface gravity and metallicity are largely degenerate as far as near-IR spectral fitting is concerned, which adds another layer of uncertainty to the parameters derived for such objects to date.

Since the low-temperature extreme of the brown dwarf regime is of particular interest for determining the form of the substellar initial mass function (e.g. Burgasser 2004), it is extremely desirable that atmospheric models in this regime are robustly constrained. Furthermore, the sub-600 K temperature regime overlaps with the warm-exoplanet regime, and such cool brown dwarfs provide excellent laboratories for improving the substellar atmospheric models which will be key to interpreting observations over the coming years. The discovery of T8+ dwarfs in binary systems with stellar primaries is of central importance for improving the current generation of atmospheric models, since we can use the properties of the primary star as fiducial constraints on the properties of the substellar secondary (e.g. Burgasser, Kirkpatrick & Lowrance 2005; Pinfield et al. 2006).

The term 'benchmark' is broadly applied to objects for which at least some properties may be determined with minimal reference to models (although the degree of reference to models that is required to determine their properties varies). With the exception of a few T dwarfs whose ages and metallicities may be gleaned from studies of the young clusters or moving groups of which they are members (e.g. Hyades; Bouvier, Kendall & Meeus 2009), the majority of T dwarf benchmarks have been found in binary systems. Indeed, one of the first unequivocally confirmed brown dwarfs, Gl229B (Nakajima et al. 1995), was found as a companion of an early-type M dwarf, studies of which have yielded improved constraints on the system properties (Leggett et al. 2002). Other notable T dwarfs in such systems include HN PegB (T2.5 ± 0.5) and HD 3651B (T7.5 ± 0.5) (Mugrauer et al. 2006; Luhman et al. 2007), which are companions to well-studied main-sequence stars (G0V and K0V, respectively).

The multiple systems Gl 570 (K4V, M1.5V, M3V and T7.5; Burgasser et al. 2000; Geballe et al. 2001) and ϵ Indi (K4.5V, T1 and T6; Scholz et al. 2003; McCaughrean et al. 2004) also have well-constrained ages from studies of the K and M dwarf members

of the systems. The ϵ Indi Ba, Bb system offers the prospect of dynamical mass estimates for the T dwarf components through direct observation of the orbital motion within its short, ~15 years, period (McCaughrean et al. 2004).

Liu, Dupuy & Ireland (2008) have suggested that brown dwarf binaries with dynamical mass determinations can serve as benchmark systems with comparable, or better, constraints on the brown dwarf gravities than in the case of wide companions of known age. They have demonstrated this approach with the first mass determination for a T dwarf binary, the T5+T5.5 system 2MASS 1534-2952AB, though the long orbital periods (>10 years) mean that some patience will be needed until a larger sample of this type of benchmark is available.

We report here on the discovery of a T8+ object, identified as a low-mass companion to the M4 dwarf Wolf 940, and explore its potential use as a benchmark object.

2 A NEW T8+ DWARF

Our searches of the UKIDSS LAS (see Lawrence et al. 2007) have been successful at identifying late-type T dwarfs (e.g. Warren et al. 2007; Lodieu et al. 2007b; Burningham et al. 2008; Pinfield et al. 2008). Using the same search methodology as previously described in detail in Pinfield et al. (2008), we identified ULAS J214638.83−001038.7 (ULAS 2146) as a candidate very late T dwarf, with *YJH* colours reminiscent of other T8+ dwarfs (it was undetected in *K*). The source was observed as part of the LAS in *YJHK* for 40 s in each filter (see Lawrence et al. 2007), and the results of these observations are summarized in Table 1. The subsequent photometric and spectroscopic follow-ups, which resulted in its classification as a T8.5 dwarf, are described in the following sections. Fig. 1 shows a UKIDSS *J*-band finding chart for this object.
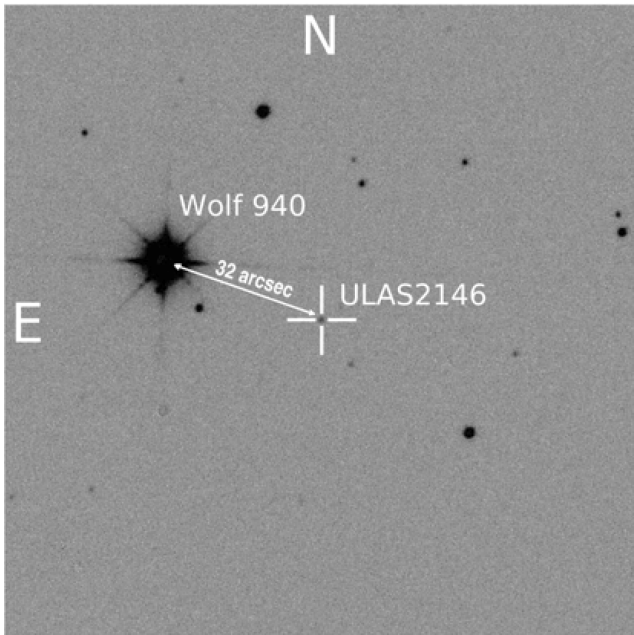
2.1 Near-infrared photometry

Near-IR follow-up photometry was obtained using the UKIRT Fast Track Imager (UFTI; Roche et al. 2003) mounted on UKIRT, and the Long-slit Infrared Imaging Spectrograph (LIRIS; Manchado et al. 1998) mounted on the William Herschel Telescope on La Palma. Image mosaics were produced using sets of jittered images, with individual exposure times, jitter patterns and number of repeats

Table 1. Summary of the near-IR photometric follow-up.

Filter	Magnitude	Instrument	UT date	Total integration time (s)	t_{int} breakdown	Photometric?
z_{EFOSC2}	22.15 ± 0.13	EFOSC2	2008 October 08	3600	($j = 1, r = 6, t_{exp} = 600$ s)	n
Y	19.02 ± 0.08	WFCAM	2007 October 12	40	($j = 2, r = 1, t_{exp} = 40$ s)	y
Y	18.97 ± 0.03	LIRIS	2008 September 15	1000	($j = 5, r = 5, t_{exp} = 40$ s)	y
J	18.02 ± 0.06	WFCAM	2007 October 12	40	($m = 4, j = 2, r = 1, t_{exp} = 5$ s)	y
J	18.21 ± 0.03	UFTI	2008 July 01	300	($j = 5, r = 1, t_{exp} = 60$ s)	y
J	18.16 ± 0.02	LIRIS	2008 September 15	600	($j = 5, r = 3, t_{exp} = 40$ s)	y
J	18.16 ± 0.02	LIRIS	2008 September 17	1200	($j = 5, r = 6, t_{exp} = 40$ s)	n
H	18.38 ± 0.20	WFCAM	2007 October 06	40	($j = 4, r = 1, t_{exp} = 10$ s)	y
H	18.77 ± 0.03	UFTI	2008 July 01	900	($j = 5, r = 3, t_{exp} = 60$ s)	y
K	18.85 ± 0.05	UFTI	2008 July 24	900	($j = 9, r = 2, t_{exp} = 60$ s)	y
K	19.08 ± 0.06	LIRIS	2008 September 15	1800	($j = 5, r = 18, t_{exp} = 20$ s)	y
L'	15.38 ± 0.11	NIRI	2008 October 20	1730	($j = 4, r = 22.5, t_{exp} = 24 \times 0.8$ s)	y

Note. The breakdown of each integration is given in the final column with the following notation: m = number of microsteps; j = number of jitter points; r = number of repeats for jitter pattern; t_{exp} = exposure time at each jitter point.

Figure 1. A 2×2 arcmin^2 J-band finding chart for ULAS 2146 taken from the UKIDSS data base.

given in Table 1. The data were dark-subtracted, flat-field-corrected, sky-subtracted and mosaicked using ORAC-DR for the UFTI data and LIRIS-DR for the LIRIS data.

We calibrated our UFTI observations using UKIRT Faint Standards (Leggett et al. 2006), with a standard observed at a similar airmass for each target. All UFTI data were obtained under photometric conditions, with seeing better than 0.9 arcsec. Photometry was performed using apertures with radii approximately $\sqrt{3}$ times the seeing, which was stable between standard star and target frames to within less than 0.5 pixel (0.045 arcsec).

The wider field LIRIS data were obtained in a mixture of photometric conditions with stable seeing, and thin cirrus in variable seeing (0.8–1.2 arcsec). Absolute photometry for ULAS 2146, and for a number of fiducial stars, was obtained during photometric conditions and calibrated using a UKIRT Faint Standard star (FS29) observed at a similar airmass. The zero-points for observations obtained in non-photometric conditions were then determined using these fiducial stars.

We used the spectra of T dwarf spectral standards for types T2–T9 to synthesise a transformation between the LIRIS Y-band filter and the MKO Y-band filter as a function of ST. We find that

$$Y_{MKO} = Y_{LIRIS} - (0.022 \times ST) - 0.089,$$

with a scatter of ± 0.01 (where ST $= 2, 3, 4$, etc. for T2, T3, T4, etc.). For earlier type stars (e.g. standards with $Y - J \sim 0$), we find that the transformation between the two filters is negligible. All Y-band magnitudes presented here were either measured in or transformed into Y_{MKO}. LIRIS uses a K_s filter, and we transformed the standard star's K magnitude to K_s using the relations of Carpenter (2001). The K_s magnitude for ULAS 2146 was transformed to the MKO system using the transform derived by Pinfield et al. (2008). In both the cases of the Y and the K bands, transforms were applied using a ST of T8.5 for ULAS 2146 (see Section 2.4).

We obtained multiple observations of ULAS 2146 in several bands to assess any level of variability. Table 1 summarizes our photometry for ULAS 2146. It can be seen that the J band is stable

to 5 per cent over time-scales of up to a year, with the exception of the UKIDSS survey magnitude (which is ~ 15 per cent brighter). We do not consider that the $\sim 2\sigma$ discrepancies between the follow-up data and the UKIDSS/WFCAM data are significant. The K-band follow-up data, however, do not agree well, and could reflect some underlying variability. However, the latter measurement derives from a LIRIS observation, and although the conversion to MKO has been well characterized for earlier STs, this may not be the case for T8+ dwarfs. As such, we defer any detailed discussion of this discrepancy until multiple measurements on the same system have been obtained. Overall, we consider that our observations are consistent with a source that is stable at the $\lesssim 5$ per cent level.

2.2 Optical photometry

We have also obtained optical z-band photometry using the ESO (European Southern Observatory) Faint Object Spectrograph and Camera (EFOSC2) mounted on the New Technology Telescope at La Silla, Chile, under programme 082.C-0399. These observations are summarized in Table 1. For this optical follow-up, we used a gunn z-band filter (ESO Z#623). The data were reduced using standard IRAF packages, and then multiple images of the target were aligned and stacked to increase signal-to-noise ratio.

We synthesised Sloan i' (AB), z' (AB) and EFOSC2 Gunn z photometry for stars with STs between B1V and M4V using spectra drawn from Gunn & Stryker (1983). The resulting synthetic colours were then used to derive the transform

$$z_{EFOSC2}(AB) = z'(AB) - 0.08[i'(AB) - z'(AB)].$$

This allowed the zero-point in our images to be determined by using SDSS stars as secondary calibrators. The uncertainty we quote for our z-band photometry incorporates a scatter of $\sim \pm 0.05$ in the determined zero-points. The results of our ground-based follow-up photometry are given in Table 1, which also gives the original WFCAM survey photometry. In all cases we take the measurement with the lowest uncertainty as our 'final' value for use elsewhere in this paper.

2.3 L'-band photometry

L'-band imaging of ULAS 2146 was obtained using the Near InfraRed Imager and Spectrometer (NIRI; Hodapp et al. 2003) on the Gemini North Telescope on Mauna Kea under programme GN-2008B-Q-29 on the night of the 2008 October 20 under photometric conditions. Individual images were made up of 24 coadded 0.8 s exposures, which were repeated over a four-point offset pattern. In total 90 images were recorded for ULAS 2146, with a further eight images obtained of the faint standard HD201941. Each image had its temporally closest neighbour subtracted from it to remove the rapidly varying and structured sky background. The sky-subtracted images were then flat-fielded using a flat-field frame constructed by median stacking the entire set of images of ULAS 2146. The resulting images were offset to the position of the first image, and median combined to produce the final image. These observations, and the resulting L'-band magnitude, are summarized in Table 1.

2.4 Near-infrared spectroscopy

Spectroscopy in the *JHK* bands was obtained for ULAS 2146 using NIRI on the Gemini North Telescope on Mauna Kea (under programme GN-2008B-Q-29). All observations were made up of a

Table 2. Summary of the near-IR spectroscopic observations.

Object	UT date	Integration time (s)	Instrument	Spectral region
ULAS 2146	2008 August 18	12×300	NIRI	J
	2008 August 21	12×300	NIRI	H
	2008 August 23	16×224	NIRI	K

set of subexposures in an ABBA jitter pattern to facilitate effective background subtraction, with a slit width of 1 arcsec. The length of the A–B jitter was 10 arcsec. The observations are summarized in Table 2.

The NIRI observations were reduced using standard IRAF Gemini packages. A comparison argon arc frame was used to obtain a dispersion solution, which was applied to the pixel coordinates in the dispersion direction on the images. The resulting wavelength-calibrated subtracted AB pairs had a low level of residual sky emission removed by fitting and subtracting this emission with a set of polynomial functions fit to each pixel row perpendicular to the dispersion direction, and considering pixel data on either side of the target spectrum only. The spectra were then extracted using a linear aperture, and cosmic rays and bad pixels removed using a sigma-clipping algorithm.

Telluric correction was achieved by dividing the extracted target spectra by that of the F4V star HIP103801, observed just before the target, in the case of the J- and H-band spectra, whilst for the K band the A0V star HIP 112179 was used. Prior to division, hydrogen lines were removed from the standard star spectrum by interpolating the stellar continuum. Relative flux calibration was then achieved by multiplying through by a blackbody spectrum with $T_{\mathrm{eff}} = 6700$ K for the F4V standard and 10 400 K for the A0V standard. Data obtained for the same spectral regions on different nights were coadded after relative flux calibration, each weighted by their exposure time.

The spectra were then normalized using the measured near-IR photometry to place the spectra on an absolute flux scale. The UFTI *JHK* photometry was used for this purpose since all three bands were obtained on the same instrument, with MKO filters, within the shortest interval available in our data for all three bands (see Table 1). The normalized spectrum was rebinned by a factor of 3 to increase the signal-to-noise ratio, whilst avoiding undersampling of the spectral resolution. The resultant *JHK* spectrum for ULAS 2146 is shown in Fig. 2.

To derive a ST for ULAS 2146, we follow the method outlined in Burningham et al. (2008) for very late T dwarfs. Fig. 3 shows the normalized *J*-and *H*-band[1] spectra of ULAS 2146 compared to those for the T8 and T9 spectral templates (Burgasser et al. 2006; Burningham et al. 2008). It can be seen from the trace of the residuals between the template spectra and those of ULAS 2146 that the latter appears to be intermediate between the two STs.

The T dwarf ST indices for ULAS 2146 are given in Table 3. In Fig. 4, we reproduce Fig. 7 from Burningham et al. (2008), with the ST indices for ULAS 2146 indicated along with those of previously published T6–T9 dwarfs. As discussed in Burningham et al. (2008), the H_2O–J, CH_4–J and CH_4–H indices are largely degenerate with type for T8 and T9 dwarfs, whilst the NH_3–H is not yet well understood. As such, we base our classification on the H_2O–H and W_J indices. It can be seen that the values for its indices

---

[1] Normalized to unity at 1.27 and 1.58 μm, respectively.

Figure 2. The NIRI *JHK* spectrum for ULAS 2146.

are consistent with classification between T8 and T9, we assign it the type T8.5 (± 0.5 subtypes).
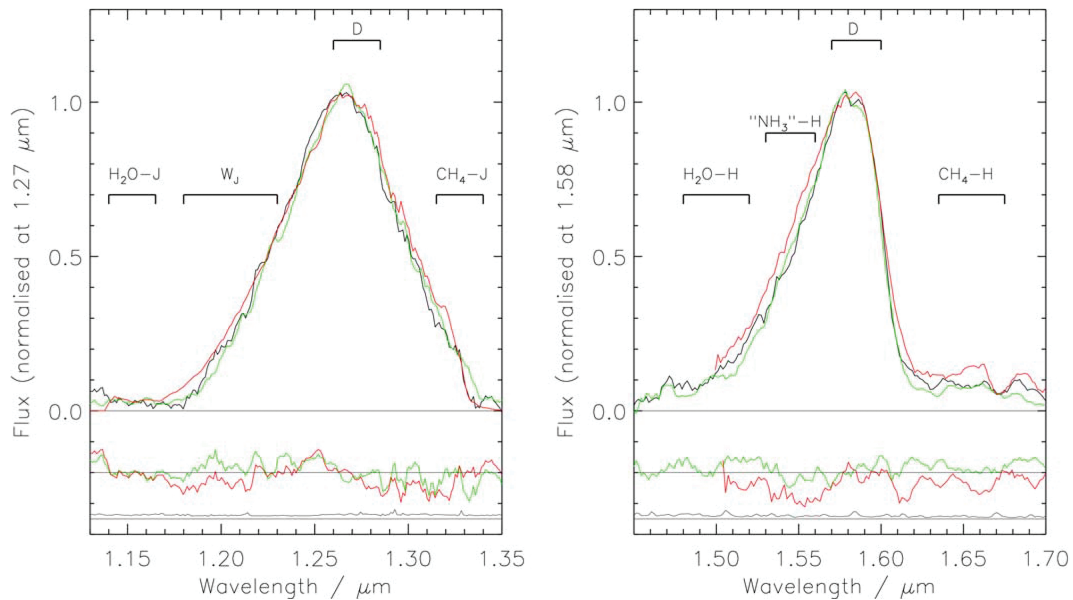
2.5 Keck laser guide star adaptive optics imaging

To search for possible unresolved binarity, we imaged ULAS 2146 on 2008 November 03 UT using the laser guide star adaptive optics (LGS AO) system (van Dam et al. 2006; Wizinowich et al. 2006) of the 10-m Keck II Telescope on Mauna Kea, Hawaii. Conditions were photometric with average seeing. We used the facility IR camera NIRC2 with its wide field-of-view camera, which produces an image scale of 39.69 ± 0.05 mas pixel^{-1}. The LGS provided the wavefront reference source for AO correction, with the exception of tip-tilt motion. Tip-tilt aberrations and quasi-static changes in the image of the LGS as seen by the wavefront sensor were measured contemporaneously with a second, lower bandwidth wavefront sensor monitoring the $R = 11.5$ mag nearby star Wolf 940, located 32 arcsec away from ULAS 2146. The sodium laser beam was pointed at the centre of the NIRC2 field of view for all observations.

We obtained a series of dithered images, offsetting the telescope by a few arcseconds, with a total integration time of 360 s. We used the *CH*4*s* filter, which has a central wavelength of 1.592 μm and a width of 0.126 μm. This filter is positioned around the *H*-band flux peak emitted by late-T dwarfs (see Tinney et al. 2005). The images were reduced in a standard fashion. We constructed flat-fields from the differences of images of the telescope dome interior with and without continuum lamp illumination. Then, we created a master sky frame from the median average of the bias-subtracted, flat-fielded images and subtracted it from the individual images. Images were registered and stacked to form a final mosaic, with a full width at half-maximum of 0.10 arcsec. No companions were detected in a 5×5 arcsec^2 region centred on ULAS 2146.

We determined upper limits on the brightness of potential companions from the direct imaging by first convolving the final mosaic with an analytical representation of the point spread function's radial profile, modelled as the sum of multiple elliptical Gaussians. We then measured the standard deviation in concentric annuli centred on the science target, normalized by the peak flux of the targets and adopted 10σ as the flux ratio limits for any companion. These limits were verified with implantation of fake companions into the image using translated and scaled versions of the science target.

Figure 3. The *J*- and *H*-band spectra of ULAS 2146 (black line) compared to those of the T8 and T9 spectral standards 2MASS 0415 (red line) and ULAS 1335 (green line), respectively (Burningham et al. 2008). The numerators for the flux ratios given in Table 3 are indicated, with the denominators marked with a 'D'. The standard spectra have been resampled to the same scales as ULAS 2146, and the spectra have been smoothed with a smoothing length of 5 pixel. The *J*- and *H*-band spectra for 2MASS 0415 have been taken from McLean et al. (2003). The single black line in the lowest panel indicates the uncertainty spectrum for ULAS 2146. The red and green lines in the middle panel indicate the residuals between ULAS 2146 and the spectra of 2MASS 0415 and ULAS 1335, respectively.

Table 3. The spectral flux ratios for ULAS 2146. Those used for spectral typing are indicated in Fig. 3.

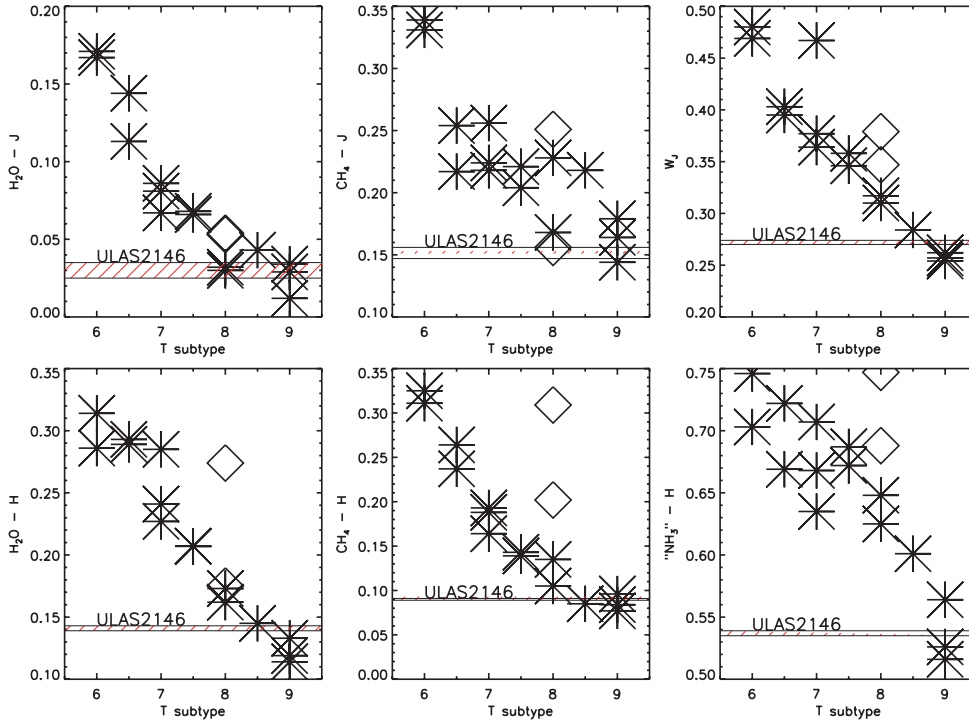| Index	Ratio	Value	Type
H_2O–J	$\dfrac{\int_{1.14}^{1.165} f(\lambda)\mathrm{d}\lambda}{\int_{1.26}^{1.285} f(\lambda)\mathrm{d}\lambda}$	0.030 ± 0.005	$\geq$T8
CH_4–J	$\dfrac{\int_{1.315}^{1.34} f(\lambda)\mathrm{d}\lambda}{\int_{1.26}^{1.285} f(\lambda)\mathrm{d}\lambda}$	0.152 ± 0.005	$\geq$T8
W_J	$\dfrac{\int_{1.18}^{1.23} f(\lambda)\mathrm{d}\lambda}{2\int_{1.26}^{1.285} f(\lambda)\mathrm{d}\lambda}$	0.272 ± 0.002	T9
H_2O–H	$\dfrac{\int_{1.48}^{1.52} f(\lambda)\mathrm{d}\lambda}{\int_{1.56}^{1.60} f(\lambda)\mathrm{d}\lambda}$	0.141 ± 0.002	T8/T9
CH_4–H	$\dfrac{\int_{1.635}^{1.675} f(\lambda)\mathrm{d}\lambda}{\int_{1.56}^{1.60} f(\lambda)\mathrm{d}\lambda}$	0.091 ± 0.002	$\geq$T8
NH_3–H	$\dfrac{\int_{1.53}^{1.56} f(\lambda)\mathrm{d}\lambda}{\int_{1.57}^{1.60} f(\lambda)\mathrm{d}\lambda}$	0.537 ± 0.002	–
CH_4–K	$\dfrac{\int_{2.215}^{2.255} f(\lambda)\mathrm{d}\lambda}{\int_{2.08}^{2.12} f(\lambda)\mathrm{d}\lambda}$	0.073 ± 0.013	–

Fig. 5 presents the final upper limits on any companion. We employed the COND models of Baraffe et al. (2003) to convert the limits into companion masses, for an assumed age of 5 Gyr and a distance estimate of 12.5 pc (see Section 3). We assumed that any cooler companion would have similar ($CH4s − H$) colours to ULAS 2146.
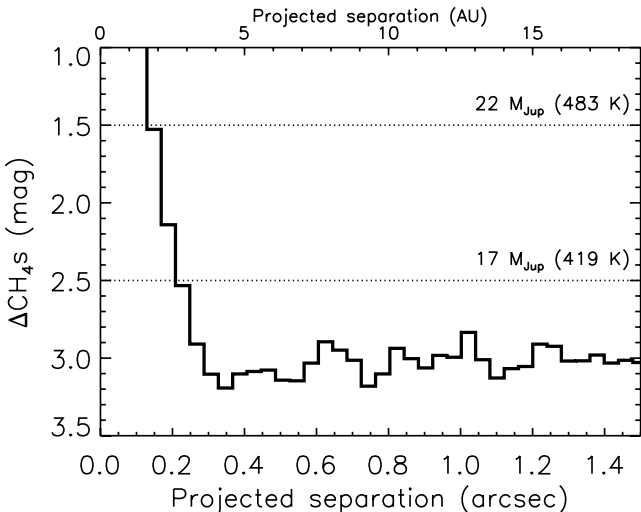
2.6 Proper motion

The photometric follow-up observations that were carried out for ULAS 2146 provided a second and third epoch of imaging data, showing the position of the source 0.72 and 0.93 years after the original LAS image was measured. Although the second epoch data cover only a relatively small area of sky (the UFTI mosaic is 135 arcsec on each side), we were able to accurately measure the positions of eight reference stars spread throughout the image, and match these to their counterparts measured in the LAS images. We used the same set of reference stars for the LIRIS data.

We used the IRAF task GEOMAP to derive spatial transformations from the UFTI and LIRIS *J*-band images into the LAS *J*-band image in which ULAS 2146 is well detected. The transform allowed for linear shifts and rotation, although the rotation that was required was negligible. We then transformed the UFTI and LIRIS pixel coordinates of ULAS 2146 into the LAS images using GEOXYTRAN, and calculated its change in position (relative to the reference stars) between the epochs. The rms scatter in the difference between the transformed positions of the reference stars and their actual measured positions was ∼±0.2 pixel for the UFTI data and ∼±0.3 pixel for the LIRIS data (corresponding to 0.04 and 0.06 arcsec in the *J*-band LAS image). Assuming that the cardinal axes of the UKIDSS LAS image are aligned perfectly with the celestial α, δ axes, we thus determined the proper motion (neglecting parallax) to be $\mu_{\alpha\cos\delta} = 895 \pm 72\,\mathrm{mas\,yr^{-1}}$ and $\mu_\delta = -538 \pm 72\,\mathrm{mas\,yr^{-1}}$. These uncertainties likely represent an underestimate, since they do not include any systematic effect that may be present in data such as these that were not initially optimized for astrometric use.

As described in Section 3, ULAS 2146 appears to be a common proper motion companion to the M4 dwarf Wolf 940, which lies at a distance of $12.50^{+0.75}_{-0.67}$ pc. We have thus repeated our proper motion determination incorporating into the solution the

Figure 4. Spectral index versus T-subtype for T6–T9 dwarfs. Asterisks indicate 'normal' dwarfs, whilst the diamonds indicate two T8p dwarfs: ULAS1017 and 2MASS J07290002−3954043. Index values for these objects are drawn from Burgasser et al. (2006), Warren et al. (2007), Delorme et al. (2008a), Looper, Kirkpatrick & Burgasser (2007) and Burningham et al. (2008) or are calculated from the objects' spectra supplied by these authors. Uncertainties in the indices are smaller than the symbol sizes, whilst the uncertainties in the STs are typically <0.5 subtypes. The index values for ULAS 2146 are indicated with hatched horizontal regions whose height is indicative of the uncertainties.

Figure 5. Limits on multiplicity of ULAS 2146 based on our Keck LGS AO imaging with the *CH*4*s* (1.59 μm) filter and theoretical models of Baraffe et al. (2003). The masses and T_{eff} corresponding to hypothetical companions are shown by the dotted horizontal lines, assuming an age of 5 Gyr.

effect of the 79.8 ± 4.5 mas parallax measured for Wolf 940 (Harrington & Dahn 1980). Our revised proper motion estimate for ULAS 2146 is thus $\mu_{\alpha\cos\delta} = 771 \pm 82$ mas yr^{-1} and $\mu_\delta = -585 \pm 82$ mas yr^{-1}, which incorporates additional uncertainty introduced by the measured parallax. For reasons discussed in Section 3, we

consider this latter proper motion estimate as our final value (see also Table 5).

3 A WIDE BINARY SYSTEM

A visual comparison between the LAS imaging data and older Schmidt plate images of the region around ULAS 2146 revealed the presence of a high-proper-motion star just 32 arcsec away from the T dwarf. This neighbouring source was identified (using the SIMBAD data base at CDS) as Wolf 940, a nearby (12.5 pc) M4 dwarf with a total proper motion of 970 mas yr^{-1}. The properties of this dwarf are given in Table 4, and it can be seen that Wolf 940 and ULAS 2146 have proper motions that agree to within 1.0σ. In order to establish if this pair is a genuine physical binary system (as might be inferred from their common proper motion), we have calculated the expected number of high-proper-motion stars that might masquerade as common proper motion companions to LAS very late T dwarf discoveries.

Including ULAS 2146, there are now five T8+ dwarfs known with T_{eff} estimates ranging down to ~550–600 K. Only ULAS 2146 is known to have a common proper motion companion. In general, these objects all have $J \simeq 18$, and we can thus consider ULAS 2146 as a typical example. Distance constraints can be estimated based on ST and magnitude, ignoring at this stage the association with Wolf 940. A typical T8 dwarf has $M_J = 16.26 \pm 0.37$ (Liu et al. 2006) and $T_{eff} \simeq 750$ K (e.g. Saumon et al. 2007), which provides a useful upper limit for a dwarf with T8.5 ± 0.5 ST. Models (e.g. Baraffe et al. 2003) suggest that 750–550 K objects could have $M_J \sim 19$ (dependent on age, mass and radius), and for $M_J = 15.89$–19 the

Table 4. Properties of Wolf 940A.

Wolf 940A	
RA (ep = 2000 eq = 2000)	21 46 40.47
Dec. (ep = 2000 eq = 2000)	−00 10 25.4
RA (ep = 2007.78 eq = 2000)	21 46 40.89[a]
Dec. (ep = 2007.78 eq = 2000)	−00 10 29.5[a]
$PM_{\alpha\cos\delta}$	765 ± 2 mas yr^{-1} [b]
PM_{δ}	−497 ± 2 mas yr^{-1} [b]
Spectral type	M4[c]
V	12.70[c]
B − V	1.61[c]
J	8.36 ± 0.02[d]
J − H	0.53 ± 0.04[d]
H − K$_s$	0.34 ± 0.04[d]
V − K$_s$	5.21
π	79.8 ± 4.5 mas[c]
Distance	$12.50^{+0.75}_{-0.67}$ pc
m-M	0.49 ± 0.13
M_{K_s}	7.00 ± 0.13
Vrad	−31.6 ± 12.2 km s^{-1} [e]
U	34.9 ± 6.1 km s^{-1} [e]
V	−49.4 ± 6.0 km s^{-1} [e]
W	−25.6 ± 9.0 km s^{-1} [e]
Galactic speed	185.3 ± 8.7 km s^{-1} [e]
[Fe/H]	−0.06 ± 0.20[f]
Mass	0.27 ± 0.03 M^f$_\odot$
H$_\alpha$EW	0.262 Å[g]
Age	3.5–6.0 Gyr[h]

[a]Epoch of the UKIDSS LAS observation.
[b]Harrington & Dahn (1980).
[c]Reid, Hawley & Gizis (1995).
[d]From 2MASS data base.
[e]Dawson & De Robertis (2005).
[f]Based on polynomial relationships (functions of $V - K_s$ and M_{K_s} from Bonfils et al. (2005).
[g]Gizis et al. (2002).
[h]Derived from activity lifetime information presented in West et al. (2008).

distance constraint for ULAS 2146 ($J = 18.21$) is 7–29 pc. However, we also allow for the possibility that such late T dwarfs could be unresolved binaries, and thus potentially 0.75 mag brighter than a single T dwarf. If $M_J = 15.14$–19, one obtains a more conservative distance constraint of 7–41 pc. Note that the known distance of Wolf 940 lies within these broad distance constraints, and thus the observable properties of ULAS 2146 (ST and brightness) are consistent with companionship.

Separations out to ∼1 arcmin from the new T8+ population and a distance range of 7–41 pc correspond to a space volume of only 0.03 pc^3. The local luminosity function measured out to distances of between 8 and 25 pc (e.g. Reid, Cruz & Allen 2007) suggests space densities of 0.06–0.11 stellar systems pc^{-3}, and thus 0.0018–0.0033 stars actually contained within this volume. However, the likelihood of finding a star that had a common proper motion decreases this number still further. We examined all *Hipparcos* stars from 7–41 pc in the direction of ULAS 2146 (±45° in RA and Dec.) and found that only three out of 619 were contained within a 200 mas yr^{-1} (∼2σ) error circle centred on the proper motion of the T dwarf. This represents a 0.48 ± 0.28 per cent probability of finding a common proper motion source by chance in such a volume. We therefore conclude that we would expect (12 ± 8) × 10^{-6} stars to masquerade as common proper motion companions to the T8+ dwarfs discovered in the UKIDSS LAS to date. This represents a

vanishingly small probability, and we thus unambiguously consider that Wolf 940 and ULAS 2146 (Wolf 940B) are a physical binary system.

3.1 The properties of Wolf 940A

This high-proper-motion M4 dwarf star was first presented by Wolf (1919), and was first recognized as a high-proper-motion object by Rodgers & Eggen (1974). Its properties are summarized in Table 4. It has a measured parallax distance of $12.50^{+0.75}_{-0.67}$ pc (Harrington & Dahn 1980), and a mass and metallicity of 0.27 ± 0.03 M$_\odot$ and −0.06 ± 0.20 dex, respectively, as estimated from fits to its M_{K_s} and $V - K$ colour using the relations presented in Bonfils et al. (2005).

The kinematics of Wolf 940 are listed in Table 4, and appear to be consistent with membership of the old disc population – kinematically defined to have an eccentricity in the ultraviolet plane <0.5 and lie outside of the young disc ellipsoid (where the young disc ellipsoid is defined as $-20 < U < +50$, $-30 < V < 0$, $-25 < W < +10$; see Eggen 1969; Leggett 1992). The Besançon Galactic population synthesis model (Robin et al. 2003) reproduces the stellar content of the Galaxy using various input physical assumptions and a simulated scenario of formation and evolution. This model has been tuned by comparison against relevant observational data as described in Haywood, Robin & Creze (1997). The disc component of the model comprises numerous subpopulations including a 3–5 Gyr population with [Fe/H] = −0.07 ± 0.18 dex. The metallicity and kinematic constraints for Wolf 940A are thus consistent with an age in the region of 3–5 Gyr. However, since such kinematic and compositional arguments apply only to populations of objects, this line of argument falls short of effectively constraining the age of Wolf 940A.

The study of M dwarf activity by Gizis, Reid & Hawley (2002) revealed that Wolf 940 has Hα in absorption, with an equivalent width of 0.262 Å. West et al. (2008) more recently demonstrated that the drop in activity fraction (as traced by Hα) as a function of the vertical distance from the Galactic plane can be explained by a combination of thin-disc dynamical heating and a rapid decrease in magnetic activity. The time-scale for this rapid activity decrease changes according to the ST, and they calibrate this via model fits to a population of 38 000 SDSS M dwarfs. For M4 dwarfs, the activity lifetime is determined to be $4.5^{+0.5}_{-1.0}$ Gyr, and we are thus able to put a lower limit of 3.5 Gyr on the age of Wolf 940A from its lack of Hα emission.

This limit comes with the caveat that the activity lifetimes were derived for a bulk population, and it is not possible to rule out variability in individual stars. Additionally, uncertainty in the ST contributes another source of uncertainty. Although the ST of Wolf 940A appears to be reliably determined, we will consider a worst case scenario to examine the impact this may have on the age limit. For example, were the ST of Wolf 940A in error by a whole subtype, and it was actually an M5 dwarf, we would find a lower limit on the age of 6.5 Gyr. Alternatively, if Wolf 940A were an M3 dwarf, the lower age limit would be 1.5 Gyr. Since the uncertainty in the ST is certainly much less than one subtype (Hawley, Gizis & Reid 1997), we adopt the limit implied by a ST of M4.

M dwarf atmospheres are too cool to produce Hα absorption in the photosphere (Cram & Mullan 1979; Pettersen & Coleman 1981), and the presence of Hα absorption thus implies the presence of a hot chromosphere (i.e. magnetic activity; Cram & Mullan 1985; Walkowicz & Hawley 2009). Therefore, the presence of Hα absorption in Wolf 940 indicates that it is still active at some level. Indeed, the relative numbers of Hα active and inactive M4 dwarfs

in SDSS suggest an M4 age no more than ∼6 Gyr. The activity age estimate for Wolf 940 is thus 3.5–6 Gyr, consistent with the indications from kinematics and metallicity.

3.2 The properties of Wolf 940B (ULAS 2146)

As a companion, Wolf 940B will share the same distance as the M4 primary ($12.50^{+0.75}_{-0.67}$ pc), and the two objects thus have a projected line-of-sight separation of 400 au. The actual semimajor axis of the binary depends on its orbital parameters. Following the method of Torres (1999), we assume random viewing angles and a uniform eccentricity distribution between $0 < e < 1$ to derive a correction factor of $1.10^{+0.91}_{-0.36}$ (68.3 per cent confidence limits) to convert projected separation into semimajor axis. At a distance of $12.50^{+0.75}_{-0.67}$ pc, this results in a semimajor axis of 440^{+370}_{-150} au. For a total mass of $0.27\,M_{\odot}$ (i.e. neglecting the mass of Wolf 940B), this corresponds to an orbital period of $18\,000^{+26\,000}_{-8000}$ yr. This is quite typical when compared to other brown dwarfs in widely separated binary systems (e.g. Burgasser et al. 2005; Pinfield et al. 2006).

It has been known for some time that the degree of multiplicity amongst very young stars is greater than that of the more evolved field star populations (Duquennoy & Mayor 1991; Leinert et al. 1993), and thus that the majority of binary systems form together in their nascent clouds. Binary components can therefore generally be assumed to share the same age and composition, and we therefore assume that Wolf 940B also has an age of 3.5–6 Gyr and a composition of [Fe/H] = -0.06 ± 0.20.

Since we have an accurate distance for Wolf 940B, we can determine its absolute magnitude; and values for M_J, M_H and M_K are given in Table 5. Fig. 6 shows M_J plotted against ST for this and other T dwarfs with reliably determined parallaxes. The very faint nature of Wolf 940B is apparent, suggestive of a very low $T_{\rm eff}$. 2MASS J0939−2448, which has recently been suggested as an equal-mass binary system with component $T_{\rm eff} \sim 600\,K$ (Burgasser et al. 2008), is indicated. The inferred $M_J = 17.67$ for the individual components of 2MASS J0939-2448 is strikingly similar to that observed for Wolf 940B.

To determine the bolometric flux, $F_{\rm bol}$, from Wolf 940B, we have combined our observed *JHK* spectra (flux calibrated using our UFTI follow-up photometry) with model spectra that allow us to estimate the flux contributions from regions shortwards and longwards of our near-IR spectral coverage. We scaled the $\lambda < 1.0\,\mu m$ portion of the model spectra to match the short-wavelength end of our *J*-band spectrum, whilst we used our *L*′-band photometry to scale the $\lambda > 2.4\,\mu m$ portion of the model spectra. We then joined them to our observed spectra and estimated the bolometric flux, assuming all flux emerges between 0.5 and 30 μm. Provided that the measured *L*′-band photometry is in a band where the level of emitted flux is relatively high (compared to the unmeasured wavelength regions) and that the theoretical models can be relied upon to provide a 'reasonable' approximation to the shape of the spectral energy distribution (cf. Roellig et al. 2004; Cushing et al. 2006; Mainzer et al. 2007), then this approach should provide valid results.

We have used the latest BT–Settl solar metallicity model spectra covering the 500–700 K temperature range, with $\log g = 4.5–5.0$, to provide the normalized shorter and longer wavelength spectral extensions to the observed near-IR spectrum. We then took the median as our final value for $F_{\rm bol}$. The scatter in values was taken as an estimate of the systematic uncertainty associated with our use of these normalized theoretical extensions. Fig. 7 shows the scaled spectra for two extremes of our theoretical extension parameter

Table 5. Properties of Wolf 940B (ULAS 2146).

Wolf 940B (ULAS 2146)	
RA (ep = 2000 eq = 2000)	21 46 38.41
Dec. (ep = 2000 eq = 2000)	−00 10 34.6
RA (ep = 2007.78 eq = 2000)	21 46 38.83[a]
Dec. (ep = 2007.78 eq = 2000)	−00 10 38.7[a]
$\mu_{\alpha\cos\delta}$	771 ± 82 mas yr^{-1}
μ_{δ}	−585 ± 82 mas yr^{-1}
Spectral type	T8.5 ± 0.5
Separation	32 arcsec
and	400 ± 22 au[b]
J	18.16 ± 0.02
$z_{\rm EFOSC2} - J$	3.99 ± 0.13
$Y - J$	0.81 ± 0.04
$J - H$	−0.61 ± 0.04
$H - K$	−0.08 ± 0.05
$J - K$	−0.69 ± 0.05
L'	15.38 ± 0.1
$K - L$	3.47 ± 0.11
Bolometric flux	1.75 ± 0.18 × 10^{-16} W m^{-2} [c]
M_J	17.68 ± 0.28[b]
M_H	18.29 ± 0.28[b]
M_K	18.37 ± 0.28[b]
$\log(L/L_{\odot})$	−6.07 ± 0.04[b]
[Fe/H]	−0.06 ± 0.20[d]
Mass	20–32 M_J [e]
Radius	0.094 ± 0.004 R[e]$_{\odot}$
$\log g$	4.75–5.00[e]
$T_{\rm eff}$	570 ± 25 K[f]

[a]Epoch of the UKIDSS LAS observation.
[b]Inferring a distance of $12.50^{+0.75}_{-0.67}$ from Wolf 940A.
[c]Integrating the measured flux from 1.0–2.4 μm and adding a theoretical correction at longer and shorter wavelength (see text).
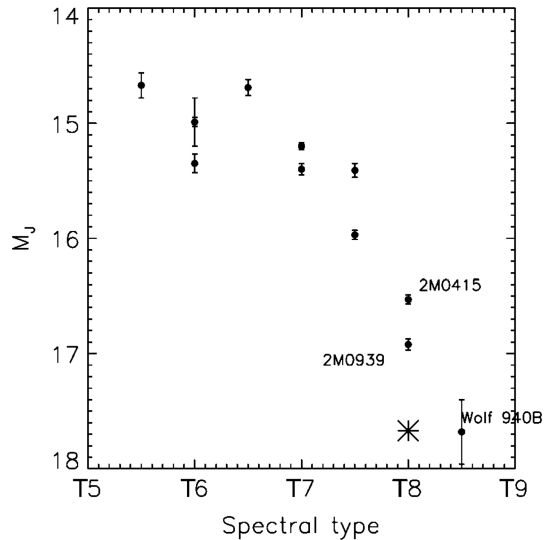[d]Inferred from Wolf 940A.
[e]Constraints derived from structure models as a function of luminosity for ages 3.5–6 Gyr.
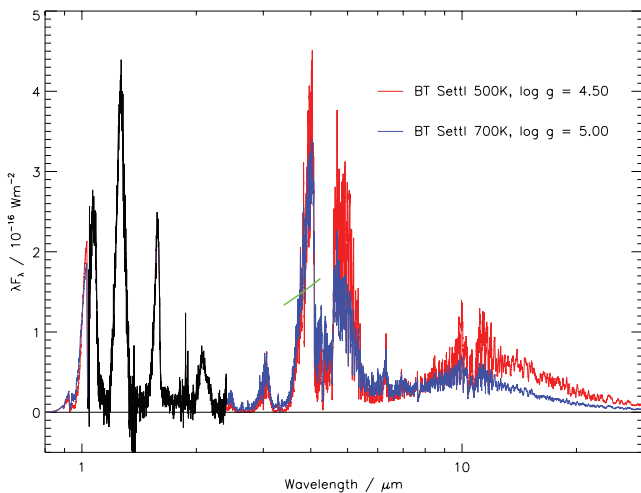[f]Derived from the luminosity and radius constraints.

space, along with our observed *JHK* spectrum for Wolf 940B. It can be seen that the optical region contributes a very small portion of the total flux (∼2 per cent), and its associated uncertainty is thus of only minor significance. Longwards of the *K* band, however, the contribution to the overall flux is greater, with ∼60 per cent of the flux emitted with $\lambda > 2.4\,\mu m$. We found that experimenting with the range of normalized theoretical spectra introduced an uncertainty of ±9 per cent. The uncertainties in our photometry used for scaling the model spectra introduced an additional ∼5 per cent uncertainty to our bolometric flux estimate, dominated by the contribution from our *L*′-band measurement. Our total uncertainty in $F_{\rm bol}$ is thus ±10 per cent, with a final value of 1.75 ± 0.18 × 10^{-16} W m^{-2}. The luminosity of Wolf 940B then comes directly from the bolometric flux and distance, allowing for uncertainties in both (see Table 5).

To place constraints on the mass and radius of Wolf 940B, we rely on theoretical structure models and infer these properties from the luminosity and age information. This requires an assumption about the multiplicity of Wolf 940B. Section 2.5 shows that Wolf 940B is unresolved at an angular resolution of 0.1 arcsec corresponding to a spatial resolution of 1.2 au at the distance of the system. So although there is evidence (Burgasser et al. 2005) that the binary fraction of brown dwarfs (as resolved at such resolutions) in widely separated stellar brown dwarf multiple systems is notably higher (45^{+15}_{-13} per cent) than that of field brown dwarfs in analogous samples

Figure 6. M_J(MKO) versus ST for T dwarfs later than T5 with parallaxes. Values of M_J have been taken from Knapp et al. (2004), whilst the STs are on the system of Burgasser et al. (2006) and Burningham et al. (2008).The three latest type T dwarfs with parallaxes and M_J(MKO) are labelled. The M_J inferred for the components of 2MASS J0939−2448 (see text and Burgasser et al. 2008) is indicated with an asterisk.

Figure 7. The NIRI *JHK* spectrum of Wolf 940B joined to scaled BT–Settl model spectra bracketing the range of parameter space considered for our F_{bol} estimate. The mean flux level implied by the L'-band photometry is indicated with a short green line.

(18^{+7}_{-4} per cent), Wolf 940B is not one of these systems. To assess the likelihood that it may be a tighter unresolved binary system, we considered the analysis of Maxted & Jeffries (2005), who use Monte Carlo simulation techniques to assess radial velocity survey data and find that a Gaussian separation distribution with a peak at 4 au and a standard deviation $\sigma_{\log(a/\mathrm{au})} = 0.6$–1.0 correctly predict the number of observed binaries (radial velocity variables). Their estimated total binary fraction is 32–45 per cent, consistent with estimates from open cluster studies (e.g. Pinfield et al. 2003; Lodieu et al. 2007a). For a Gaussian separation distribution of this type, we would expect at most a 10–20 per cent binary fraction for systems with separation <1.2 au.

The metastudy by Allennn (2007) estimates the binary fraction for objects later than M6 in the field as 20–22 per cent, using Bayesian methods, and ~6 per cent for systems with separations less than 1 au. Similarly, Joergens (2008) found a binary fraction for low-mass stars and brown dwarfs of 10–30 per cent in the Chameleon I star-forming region, with a frequency of less than 10 per cent for binary separations of <1 au.

Since the binary fraction of a magnitude-limited survey, such as UKIDSS, will be increased by unresolved binaries, which are seen to greater distances, caution must be used when assessing the likelihood of binarity for an object from such a survey. For this reason, we do not derive a formal likelihood of unresolved binarity for Wolf 940B. However, based on the results described above, it is possible to state that it is likely that Wolf 940B is a single object, and we proceed with our analysis on this basis.

Assuming evolution of the mass–luminosity and radius–luminosity relations from Baraffe et al. (2003) isochrones, we used linear interpolation (between isochrones) to derive theoretical mass and radius estimates appropriate for the measured luminosity and age constraints of Wolf 940B. These parameters (including $\log g$) are given in Table 5.
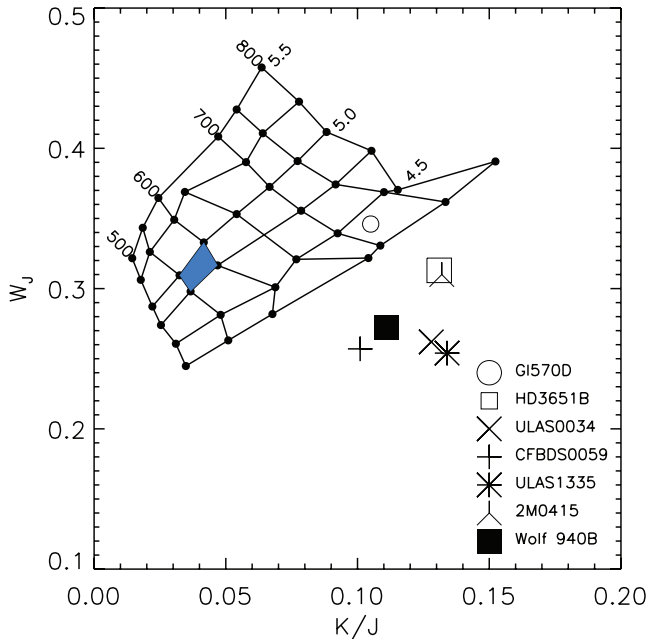
We can use our estimate of the radius and the luminosity to determine T_{eff}. However, since the radius estimate depends strongly on the assumed age, so does the derived T_{eff}. As discussed in Section 3.1, the ST that is used for Wolf 940A influences the age constraints implied by its Hα absorption. The worst case scenarios of errors of ±1 subtype in ST would lead to age ranges of 1.5–10 or 6.5–10 Gyr. The extremes of these alternatives would imply radii of 0.105 $R_{\odot}$ for an age of 1.5 Gyr and 0.084 $R_{\odot}$ for an age of 10 Gyr, and $\log g$ constraints of 4.50–5.1, respectively. Given our luminosity estimate, these extreme cases imply that $T_{eff} = 540$ and 605 K, respectively. Since the ST uncertainty is small, however, we adopt the range of values implied by the M4 classification, and the associated age estimate of 3.5–6 Gyr, in Table 5.

We thus obtain our best estimate of $T_{eff} = 570 \pm 25$ K and $\log g = 4.75$–5.00 for Wolf 940B directly from the constraints we place on the luminosity and radius of this object.
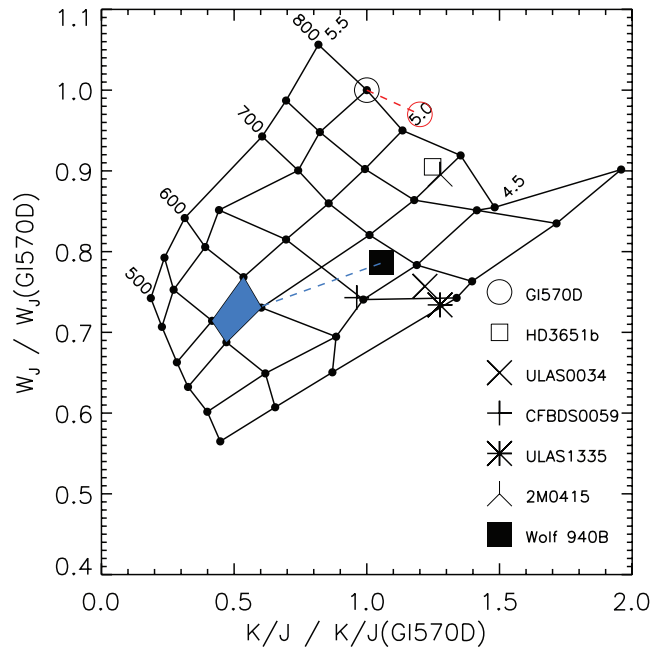
4 TESTING THE MODELS

We now use our robust properties for Wolf 940B to make a direct comparison between observation and specific theoretical model predictions. We first apply the (W_J, K/J) analysis described by Warren et al. (2007) for ULAS 0034, and since repeated for CFBDS 0059 (Delorme et al. 2008a) and ULAS 1335 (Burningham et al. 2008). In Fig. 8, we plot a grid of the W_J and K/J flux ratios for a recent set of solar metallicity BT–Settl models, along with the same ratios for a group of late T dwarfs, including three T9s, the benchmark T dwarfs HD 3651B and Gl 570D, along with the T8 dwarf 2MASS 0415. It is immediately clear that there are large differences between the model predictions and the values derived from the objects' spectra.

To assess the ability of the model spectra to make relative predictions for objects' properties, we replot the same grid in Fig. 9, however in this case we anchor the grid to values for the benchmark T dwarf Gl 570D. We have adopted the values derived by Saumon et al. (2006) of $T_{eff} = 810 \pm 10$ K and $\log g = 5.09$–5.23, and use the metallicity found by Geballe et al. (2001) of [M/H] = 0.01. For the purposes of anchoring the solar metallicity (W_J, K/J) grid, we associated Gl 570D with the model values for $T_{eff} = 800$ K and $\log g = 5.25$. Even with such correction, this diagram still fails to correctly identify the properties of Wolf 940B. The model spectra underpredict the K/J ratio in absolute terms (Fig. 8), and also predict

Figure 8. W_J versus K/J indices for a grid of the most recent set of solar metallicity BT–Settl model spectra. Flux ratios for HD 3651B were measured using the spectrum from Burgasser (2007), for 2MASS 0415 using the spectrum from Burgasser (2007) and for Gl 570D using the spectrum from Geballe et al. (2001). Those for the three T9 dwarfs ULAS 0034, CFBDS 0059 and ULAS 1335 were taken from their respective discovery papers (Warren et al. 2007; Delorme et al. 2008a; Burningham et al. 2008). The blue shading indicates the region of this grid that should contain Wolf 940B. Uncertainties are of similar size to the symbols.

Figure 9. W_J versus K/J indices for a grid of solar metallicity BT–Settl model spectra. The grid is normalized such that the model values for the T_{eff} and log g of Gl 570D lie at coordinates (1,1). All observed values of W_J and K/J are shown as a proportion of those of Gl 570D. We have indicated, with a red dotted line and open circle, the relative shift in position on the grid associated with increasing metallicity by +0.1 dex. Uncertainties are of similar size to the symbols. The blue dotted line highlights the difference between the true properties of Wolf 940B, and those expected from the model grid.

a greater decrease in its value on going from $T_{eff} = 800$ to 570 K than is observed from Gl570D and Wolf 940B (Fig. 9). In the case of the W_J value, the absolute prediction is an overestimate, whilst the predicted decrease between $T_{eff} = 800$ and 570 K is close to reality. As a result of these effects, in the case of Wolf 940B, a simple $(W_J, K/J)$ analysis would have overestimated the temperature by ∼100 K.

In Fig. 10, we plot the comparison of the observed spectrum of Wolf 940B with those of the models that bracket its derived properties, scaled for the distance of 12.5 pc and a radius 0.094 R⊙, and in Fig. 11 we plot the residuals between *JHK* model spectra and our data. The reason for the offsets in the $(W_J, K/J)$ plots is demonstrated here. The low predicted value of K/J in both the unanchored and the anchored plots appears to be driven by systematic underestimate of the *K*-band flux suggesting problems with the opacity due to collisionally induced absorption by H_2. The only model that does not underestimate the *K*-band peak is that for $T_{eff} = 600$ K, log $g = 4.75$ and [M/H] $= +0.1$. However, this model spectrum overestimates the *J*- and *H*-band peaks by the greatest extent. Since model spectra for the low-metallicity parameter space are yet to be computed, we are unable to explore the full range of possibilities for this object's metallicity. In fact, Liu, Leggett & Chiu (2007) have found that the relative changes in model spectra with metallicity do not agree very well with the available data for late T dwarfs. We thus defer a more extensive model comparison to a future paper.

Examination of the strengths of the *YJHK* flux peaks, with reference to the trends in model spectra with metallicity, gravity and temperature, is thought to be useful for identifying T dwarfs with
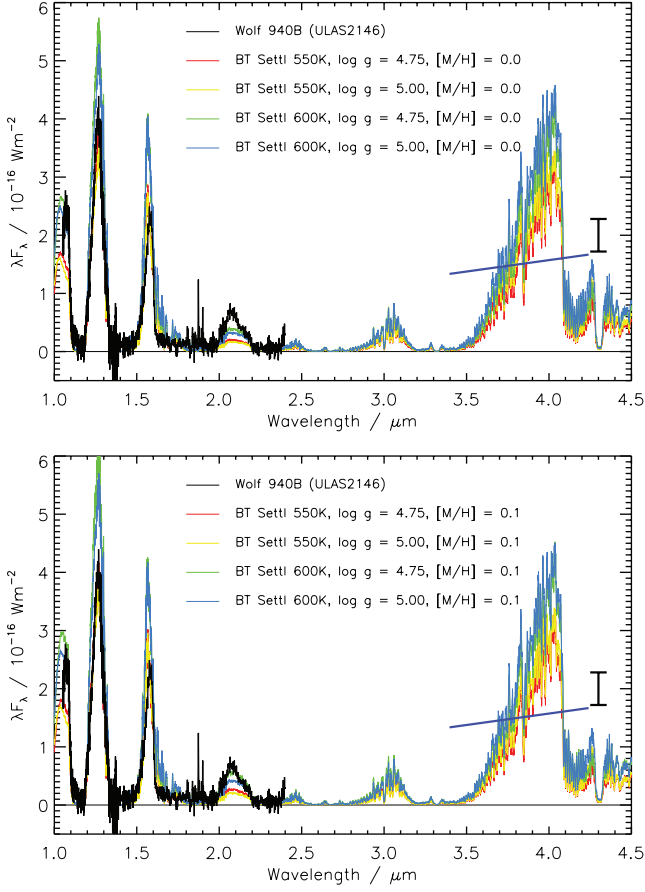
unusual properties (e.g. Pinfield et al. 2008). The well-constrained nature of Wolf 940B makes it a useful reference point for assessing such spectral sensitivities. We have calculated the *JHK* flux peak ratios for Wolf 940B, and compared them to other very late T dwarfs and the two late T benchmarks, Gl 570D and HD 3651B, in Table 6. Flux peak ratios involving the *Y*-band peak must be neglected, however, since our *JHK* spectrum for ULAS 2146 does not provide sufficient coverage.

As discussed in more detail by Pinfield et al. (2008), the most dramatic trends in the relative strengths of the flux peaks of the BT–Settl model spectra appear to be associated with varying gravity and metallicity, with *K*-band suppression (decreasing K/J) seen with increasing gravity and decreasing metallicity. The *H*-band peak is more weakly affected by varying these parameters, and has trends in the opposite sense to the *K* band, i.e. decreasing strength with decreasing gravity or metallicity (decreasing H/J). The flux peaks show a weaker response to varying T_{eff}, with *H*-band strengthening with falling T_{eff}, and the *K*-band weakening.

Direct comparison of the flux peak ratios of Wolf 940B with the other two benchmark objects in Table 6 must be rather cursory at this stage. The ∼200 K difference in T_{eff} between the objects makes it impossible to disentangle the effects of gravity/metallicity from those due to T_{eff} differences. However, it does appear that the relative ratios of the three objects are broadly consistent with their properties and the trends described above.

5 SUMMARY AND CONCLUSIONS

We have identified a T8.5 (±0.5 subtypes) dwarf in a common proper motion binary system with the M4 dwarf Wolf 940. We
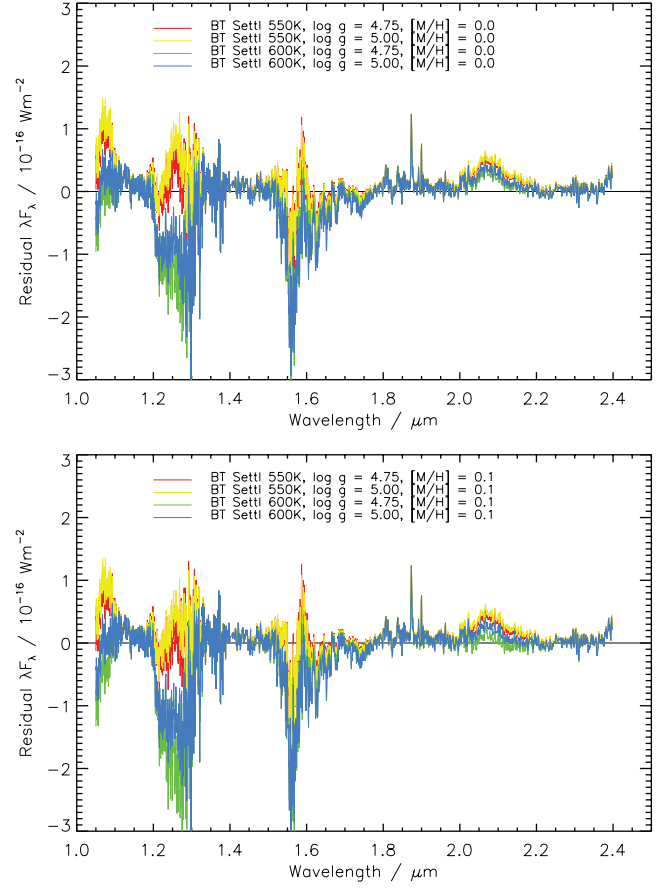
Figure 10. A comparison of BT–Settl model spectra bracketing the derived parameters for Wolf 940B with the observed spectrum. The top plot shows the comparison for solar metallicity models, whilst the bottom plot shows mildly metal-rich models. The short, straight, blue line in each case indicates the mean flux level in our L'-band photometric observation. The black error bar at the right of each plot is representative of the uncertainty in a scaled model flux of 2×10^{-16} W m^{-2} due to the uncertainties in the parallax and radius of Wolf 940B.

designate the M4 primary as Wolf 940A, and the T8.5 dwarf as Wolf 940B, which lies at a projected separation of 400 au. By using the properties of Wolf 940A to constrain those of Wolf 940B, and with reference to evolutionary structural models of Baraffe et al. (2003), we estimate that Wolf 940B has $T_{\rm eff} = 570 \pm 25$ K, $\log g = 4.75$–5.0 and [M/H] $= -0.06 \pm 0.20$. This represents the first estimate of the properties for a T8+ dwarf that does not rest on the fitting of model spectra, although we do rely on the radius predicted by evolutionary models and an age estimate from the activity of the primary of 3.5–6.0 Gyr.

Our comparison of the near-IR spectrum for Wolf 940B with the current generation of BT–Settl model spectra reveals that the strength of the K-band flux peak is underestimated by the models. This is likely the driving factor behind the $+100$ K temperature overestimate implied by (W_J, K/J) spectral ratio analysis. This indicates that $T_{\rm eff}$ determined for late T dwarfs from (W_J, K/J) analysis should be treated with extreme caution.

This system should be of significant benefit for improving understanding of <600 K atmospheres. In the near future, we expect *Spitzer* IRS spectroscopy and IRAC imaging to be obtained, which will allow a detailed examination of the predictions of a variety of very cool model spectra. Furthermore, intermediate resolution

Figure 11. The residuals between the model spectra plotted in Fig. 10 and the *JHK* spectrum of Wolf 940B.

Table 6. The flux peak ratios for other published T8+ dwarfs, along with several T8 dwarfs, and the two late T benchmarks. We have included the values for Wolf 940B from Table 3 for comparison. The ranges for each flux peak are as follows: *J*: 1.25–1.29 μm; *H*: 1.56–1.60 μm; *K*: 2.06–2.10 μm.

Object	Spectral type	*H/J*	*K/J*	*K/H*
Wolf 940B (ULAS 2146)	T8.5	0.454	0.111	0.245
ULAS 0034[1]	T9	0.475	0.126	0.266
CFBDS 0059[2]	T9	0.580	0.095	0.164
ULAS 1335[3]	T9	0.574	0.134	0.232
2MASS 0415[4]	T8	0.531	0.132	0.249
2MASS 0939[5]	T8	0.483	0.060	0.124
2MASS 0729[6]	T8p	0.447	0.093	0.207
ULAS 1017[3]	T8p	0.411	0.119	0.288
Gl 570D[7]	T7.5	0.423	0.105	0.247
HD 3651B[8]	T7.5	0.454	0.131	0.289

Note. Original publications for source spectra:
[1] Warren et al. (2007).
[2] Delorme et al. (2008a).
[3] Burningham et al. (2008).
[4] Burgasser (2004).
[5] Burgasser et al. (2006).
[6] Looper et al. (2007).
[7] Geballe et al. (2001).
[8] Burgasser (2007).

spectroscopy can be used to assess if Wolf 940B is a rapid rotator, whilst repeat observations can be used to search for close binarity via modulation of Wolf 940B's radial velocity. Finally, it is highly desirable that we improve the metallicity constraints on this system. This requires both improvement in the understanding of metallicity indicators in M dwarfs, and a more detailed study of Wolf 940A. Repeat Hα measurements for Wolf 940A will reveal if its Hα absorption is stable, thus providing an indication of the reliability of our age constraint.

REFERENCES

Allen P. R., 2007, ApJ, 668, 492
Baraffe I., Chabrier G., Barman T. S., Allard F., Hauschildt P. H., 2003, A&A, 402, 701
Bonfils X., Delfosse X., Udry S., Santos N. C., Forveille T., Ségransan D., 2005, A&A, 442, 635
Bouvier J., Kendall T., Meeus G., 2009, in Stempels E., ed., AIP Conf. Proc. Vol. 1094, Cool Stars, Stellar Systems and the Sun. Springer, Berlin, p. 497
Burgasser A. J., 2004, ApJS, 155, 191
Burgasser A. J., 2007, ApJ, 658, 617
Burgasser A. J. et al., 2000, ApJ, 531, L57
Burgasser A. J., Kirkpatrick J. D., Lowrance P. J., 2005, AJ, 129, 2849
Burgasser A. J., Geballe T. R., Leggett S. K., Kirkpatrick J. D., Golimowski D. A., 2006, ApJ, 637, 1067
Burgasser A. J., Tinney C. G., Cushing M. C., Saumon D., Marley M. S., Bennett C. S., Kirkpatrick J. D., 2008, ApJ, 689, L53
Burningham B. et al., 2008, MNRAS, 391, 320
Carpenter J. M., 2001, AJ, 121, 2851
Cram L. E., Mullan D. J., 1979, ApJ, 234, 579
Cram L. E., Mullan D. J., 1985, ApJ, 294, 626
Cushing M. C. et al., 2006, ApJ, 648, 614
Dawson P. C., De Robertis M. M., 2005, PASP, 117, 1
Delorme P. et al., 2008a, A&A, 482, 961
Delorme P. et al., 2008b, A&A, 484, 469
Duquennoy A., Mayor M., 1991, A&A, 248, 485
Eggen O. J., 1969, PASP, 81, 553
Geballe T. R., Saumon D., Leggett S. K., Knapp G. R., Marley M. S., Lodders K., 2001, ApJ, 556, 373
Gizis J. E., Reid I. N., Hawley S. L., 2002, AJ, 123, 3356
Gunn J. E., Stryker L. L., 1983, ApJS, 52, 121
Harrington R. S., Dahn C. C., 1980, AJ, 85, 454
Hawley S. L., Gizis J. E., Reid N. I., 1997, AJ, 113, 1458
Haywood M., Robin A. C., Creze M., 1997, A&A, 320, 428
Hodapp K. W. et al., 2003, PASP, 115, 1388
Joergens V., 2008, A&A, 492, 545
Knapp G. R. et al., 2004, AJ, 127, 3553
Lawrence A. et al., 2007, MNRAS, 379, 1599
Leggett S. K., 1992, ApJS, 82, 351
Leggett S. K., Hauschildt P. H., Allard F., Geballe T. R., Baron E., 2002, MNRAS, 332, 78
Leggett S. K. et al., 2006, MNRAS, 373, 781
Leggett S. K. et al., 2009, ApJ, in press
Leinert C., Zinnecker H., Weitzel N., Christou J., Ridgway S. T., Jameson R., Haas M., Lenzen R., 1993, A&A, 278, 129
Liu M. C., Leggett S. K., Golimowski D. A., Chiu K., Fan X., Geballe T. R., Schneider D. P., Brinkmann J., 2006, ApJ, 647, 1393L
Liu M. C., Leggett S. K., Chiu K., 2007, ApJ, 660, 1507
Liu M. C., Dupuy T. J., Ireland M. J., 2008, ApJ, 689, 436
Lodieu N., Dobbie P. D., Deacon N. R., Hodgkin S. T., Hambly N. C., Jameson R. F., 2007a, MNRAS, 380, 712
Lodieu N. et al., 2007b, MNRAS, 379, 1423
Looper D. L., Kirkpatrick J. D., Burgasser A. J., 2007, AJ, 134, 1162
Luhman K. L. et al., 2007, ApJ, 654, 570
McCaughrean M. J., Close L. M., Scholz R.-D., Lenzen R., Biller B., Brandner W., Hartung M., Lodieu N., 2004, A&A, 413, 1029
McLean I. S., McGovern M. R., Burgasser A. J., Kirkpatrick J. D., Prato L., Kim S. S., 2003, ApJ, 596, 561
Mainzer A. K. et al., 2007, ApJ, 662, 1245
Manchado A. et al., 1998, in Fowler A. M., ed., Proc. SPIE Conf. Vol. 3354, Infrared Astronomical Instrumentation. SPIE, Bellingham, p. 448
Maxted P. F. L., Jeffries R. D., 2005, MNRAS, 362, L45
Mugrauer M., Seifahrt A., Neuhäuser R., Mazeh T., 2006, MNRAS, 373, L31
Nakajima T., Oppenheimer B. R., Kulkarni S. R., Golimowski D. A., Matthews K., Durrance S. T., 1995, Nat, 378, 463
Pettersen B. R., Coleman L. A., 1981, ApJ, 251, 571
Pinfield D. J., Dobbie P. D., Jameson R. F., Steele I. A., Jones H. R. A., Katsiyannis A. C., 2003, MNRAS, 342, 1241
Pinfield D. J., Jones H. R. A., Lucas P. W., Kendall T. R., Folkes S. L., Day-Jones A. C., Chappelle R. J., Steele I. A., 2006, MNRAS, 368, 1281
Pinfield D. J., et al., 2008, MNRAS, 390, 304
Reid I. N., Hawley S. L., Gizis J. E., 1995, AJ, 110, 1838
Reid I. N., Cruz K. L., Allen P. R., 2007, AJ, 133, 2825
Robin A. C., Reylé C., Derrière S., Picaud S., 2003, A&A, 409, 523
Roche P. F. et al., 2003, in Iye M., Moorwood A. F. M., eds., Proc. SPIE Conf. Vol. 4841, Instrument Design and Performance for Optical/Infrared Ground-based Telescopes. SPIE, Bellingham, p. 901
Rodgers A. W., Eggen O. J., 1974, PASP, 86, 742
Roellig T. L. et al., 2004, ApJS, 154, 418
Saumon D., Marley M. S., Cushing M. C., Leggett S. K., Roellig T. L., Lodders K., Freedman R. S., 2006, ApJ, 647, 552
Saumon D. et al., 2007, ApJ, 656, 1136
Scholz R.-D., McCaughrean M. J., Lodieu N., Kuhlbrodt B., 2003, A&A, 398, L29
Tinney C. G., Burgasser A. J., Kirkpatrick J. D., McElwain M. W., 2005, AJ, 130, 2326
Torres G., 1999, PASP, 111, 169
van Dam M. A. et al., 2006, PASP, 118, 310
Walkowicz L. M., Hawley S. L., 2009, AJ, 137, 3297
Warren S. J. et al., 2007, MNRAS, 381, 1400
West A. A., Hawley S. L., Bochanski J. J., Covey K. R., Reid I. N., Dhital S., Hilton E. J., Masuda M., 2008, AJ, 135, 785
Wizinowich P. L. et al., 2006, PASP, 118, 297
Wolf M., 1919, Astron. Nachr., 209, 11

This paper has been typeset from a TeX/LaTeX file prepared by the author.